

# THE INTERNAL DYNAMICS OF GLOBULAR CLUSTERS

G. MEYLAN

*European Southern Observatory, Karl-Schwarzschild-Strasse 2,  
D-85748 Garching bei München, Germany  
E-mail: gmeylan@eso.org*

Galactic globular clusters are ancient building blocks of our Galaxy. They represent a very interesting family of stellar systems in which some fundamental dynamical processes have been taking place for more than 10 Gyr, but on time scales shorter than the age of the universe. In contrast with galaxies, these star clusters represent unique laboratories for learning about two-body relaxation, mass segregation from equipartition of energy, stellar collisions, stellar mergers, core collapse, and tidal disruption. This review briefly summarizes some of the tremendous developments that have taken place during the last two decades. It ends with some recent results on tidal tails around galactic globular clusters and on a very massive globular cluster in M31.

## 1 Introduction

There are about 150 globulars orbiting in the halo of our Galaxy. They look like huge swarms of stars, characterized by symmetry and apparent smoothness. Fig. 1 below displays an image of NGC 5139  $\equiv \omega$  Centauri, the brightest and most massive galactic globular cluster. This 40' by 40' image from the Digital Sky Survey does not reach, in spite of its rather large angular size, the outer parts of the cluster. With its tidal radius of about 40-50', the apparent diameter of  $\omega$  Centauri on the plane of the sky is significantly larger than the apparent 30' diameter of the full moon.

Globular clusters are old stellar systems, made of one single generation of stars. Although still somewhat uncertain, their individual ages range between about 10 and 15 Gyr, with possible significant differences, up to a few gigayears, from one cluster to the other. Other properties of globular clusters exhibit significant variations: e.g., their integrated absolute magnitudes range from  $M_V^{int} = -1.7$  to  $-10.1$  mag; their total masses from  $M_{tot} = 10^3$  to  $5 \times 10^6 M_\odot$ ; their galactocentric distances from 2 to 120 kpc.

## 2 A few dynamical time scales

The dynamics of any stellar system may be characterized by the following three dynamical time scales: (i) the crossing time  $t_{cr}$ , which is the time needed by a star to move across the system; (ii) the relaxation time  $t_{rlx}$ , which is the

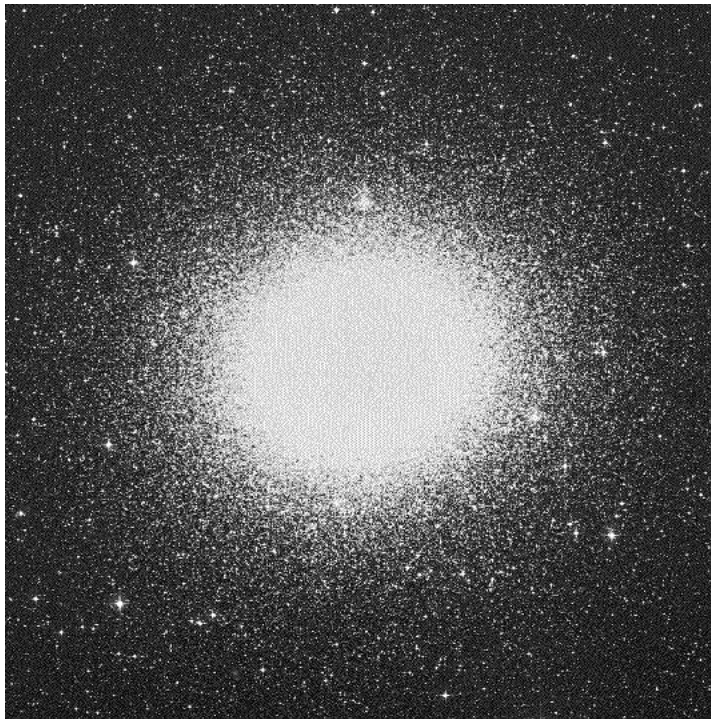


Figure 1. NGC 5139  $\equiv \omega$  Centauri is the brightest and most massive galactic globular cluster. This image, from the Digital Sky Survey, has 40' by 40' in size. North is to the top, East to the left.

time needed by the stellar encounters to redistribute energies, setting up a near-maxwellian velocity distribution; (iii) the evolution time  $t_{ev}$ , which is the time during which energy-changing mechanisms operate, stars escape, while the size and profile of the system change.

In the case of globular clusters,  $t_{cr} \sim 10^6$ yr,  $t_{rlx} \sim 100 \cdot 10^6$ yr, and  $t_{ev} \sim 10 \cdot 10^9$ yr. It is worth mentioning that several (different and precise) definitions exist for the relaxation time. The most commonly used is the half-mass relaxation time  $t_{rh}$  of Spitzer (1987, Eq. 2-62), where the values for the mass-weighted mean square velocity of the stars and the mass density are those evaluated at the half-mass radius of the system (see Meylan & Heggie 1997 for a review). It has been suggested that the combination of relaxation with the chaotic nature of stellar orbits in non-integrable potentials (e.g., most ax-

Table 1.

open clusters	$t_{cr} \sim t_{rlx} \ll t_{ev}$	quickly dissolved
globular clusters	$t_{cr} \ll t_{rlx} \ll t_{ev}$	
galaxies	$t_{cr} \ll t_{rlx} \sim t_{ev}$	not relaxed

isymmetric potentials) causes a great enhancement in the rate of relaxation (Pfenniger 1986, Kandrup & Willmes 1994). Another suggestion which, if confirmed, would revolutionise the theory of relaxation was made by Gurzadyan & Savvidy (1984, 1986) who proposed a much faster relaxation time scale than in standard theory, by a factor of order  $N^{2/3}$ . There is some support for this view on observational grounds (Vesperini 1992a,b).

From size, luminosity, and mass points of view, globular clusters are bracketed by open clusters on the lower side and dwarf elliptical galaxies on the upper side. Table 1 displays, for open clusters, globular clusters, and galaxies, some interesting relations between the above three time scales. For open clusters, crossing time  $t_{cr}$  and relaxation time  $t_{rlx}$  are more or less equivalent, both being significantly smaller than the evolution time  $t_{ev}$ . This means that most open clusters dissolve within a few gigayears. For galaxies, relaxation time  $t_{rlx}$  and evolution time  $t_{ev}$  are more or less equivalent, both being significantly larger than the crossing time  $t_{cr}$ . This means that galaxies are not relaxed, i.e., not dynamically evolved. It is only for globular clusters that all three time scales are significantly different, implying plenty of time for a significant dynamical evolution in these stellar systems, although avoiding quick evaporation.

Consequently, globular clusters represent an interesting class of dynamical stellar systems in which some dynamical processes take place on time scales shorter than their age, i.e., shorter than the Hubble time, providing us with unique dynamical laboratories for learning about two-body relaxation, mass segregation from equipartition of energy, stellar collisions, stellar mergers, and core collapse. All these dynamical phenomena are related to the internal dynamical evolution only, and would also happen in isolated globular clusters. The external dynamical disturbances — tidal stripping by the galactic gravitational field — influence equally strongly the dynamical evolution of globular clusters.

### 3 Model building for globular clusters

Already before the pioneering work of von Hoerner (1960), who made the first  $N$ -body calculations with  $N = 16$ , it was realized that computation of individual stellar motions could be replaced by statistical methods. Some parallels were drawn between a molecular gas and star clusters: the stars were considered as mass points representing the molecules in a collisionless gas. The analogy between a gas of molecules and a gas of stars is subject to criticisms, since the mean free path of a molecule is generally quite small compared with the size or scale height of the system, whereas the mean free path of a star is much larger than the diameter of the cluster; in addition molecules travel along straight lines, while stars move along orbits in the gravitational potential of all the other stars of the stellar system. Stellar collisions in clusters were studied by Jeans (1913), who remarked that they might be important in such stellar systems. The problem was then to seek the possible spherical distribution of such a gas in a steady state.

#### 3.1 Boltzmann's equation

The commonest way of defining a model of a star cluster is in terms of its distribution function  $f(\mathbf{r}, \mathbf{v}, m)$ , which is defined by the statement that  $f d^3\mathbf{r} d^3\mathbf{v} dm$  is the mean number of stars with positions in a small box  $d^3\mathbf{r}$  in space, velocities in a small box  $d^3\mathbf{v}$  and masses in an interval  $dm$ . In terms of this description a fairly general equation for the dynamical evolution is Boltzmann's equation,

$$\frac{\partial f}{\partial t} + \mathbf{v} \cdot \nabla_{\mathbf{r}} f - \nabla_{\mathbf{r}} \Phi \cdot \nabla_{\mathbf{v}} f = \frac{\partial f}{\partial t}_{enc}, \quad (1)$$

where  $\Phi$  is the smoothed gravitational potential per unit mass, and the right-hand side describes the effect of two-body encounters. The distribution  $f$  is a function of 7 variables if we take into account time. This is rather more than can be handle. But it is possible to reduce the complexity posed by Boltzmann's equation by taking moments.

By taking moments of the Boltzmann's equation with respect to velocities we obtain, for  $n = 0$  and 1, the Jeans equations which are expressions describing the rotation and the velocity dispersion:

$$\int \text{Boltzmann} \cdot v_j^n d^3\mathbf{v} = \text{JeansEqu}. \quad (2)$$

By taking moments of the Jeans equations with respect to positions, we obtain the Tensor Virial equations which are expressions relating the global

kinematics to the morphology of the system, e.g., the ratio  $v_o/\sigma_o$  of ordered to random motions:

$$\int Jeans \cdot x_j^n d^3\mathbf{x} = Tensor\ Virial \quad (3)$$

In these ways, we obtain information about the general properties of solutions of Boltzmann's equation without recovering any solutions.

### 3.2 *Liouville's equation and Jean's theorem*

The general Boltzmann's equation can be greatly simplified in other ways. Because  $t_{cr}$  is so short, after a few orbits the stars are mixed into a nearly stationary distribution, and so the term  $\partial f/\partial t$  is practically equal to zero. In a similar way, because  $t_{rh}$  is so long, the collision term  $(\partial f/\partial t)_{enc}$  can be ignored. What is left, i.e.,

$$\mathbf{v} \cdot \nabla_{\mathbf{r}} f - \nabla_{\mathbf{r}} \Phi \cdot \nabla_{\mathbf{v}} f = 0, \quad (4)$$

is an equilibrium form of what is frequently called Liouville's equation, or the collisionless Boltzmann's equation, or the Vlasov equation.

In simple cases, the general solution of Equ. 4 is given by Jeans' theorem, which states that  $f$  must be a function of the constants of the equations of motion of a star, e.g., of the stellar energy per unit mass  $\varepsilon = v^2/2 + \Phi$ . Such quantities are also called integrals of the motion. If not all integrals of the motion are known, such functions are still solutions, though not the most general. For a self-consistent solution, the distribution function  $f$  must correspond to the density  $\rho$  required to provide the cluster potential  $\Phi_c$ , i.e.:

$$\nabla^2 \Phi_c = 4\pi G \rho = 4\pi G \int m f d^3\mathbf{r} d^3\mathbf{v} dm. \quad (5)$$

Many different kinds of models may be constructed with this approach. In the first place there is considerable freedom of choice over which integrals of the motion to include. In the second place one is free to choose the functional dependence of these integrals, i.e., the analytic form of the distribution function (see, e.g., Binney 1982, and Binney & Tremaine 1987).

King (1966) provided the first grid of models (with different concentrations  $c = \log(r_t/r_c)$  where  $r_t$  and  $r_c$  are the tidal and core radii, respectively) that incorporate the three most important elements governing globular cluster structure: dynamical equilibrium, two-body relaxation, and tidal truncation. These models depend on one integral of the motion only — the stellar energy per unit mass  $\varepsilon$  — and the functional dependence is based on the lowered

maxwellian (see Equ. 6 below). Such models are spherical and their velocity dispersion tensor is everywhere isotropic.

Models more complicated have been built since then. Da Costa & Freeman (1976) generalized the simple single-mass King models to produce more realistic multi-mass models with full equipartition of energy in the centre. Gunn & Griffin (1979) developed multi-mass models whose distribution functions depend on the stellar energy per unit mass  $\varepsilon$  and the specific angular momentum  $l$ . Such models are spherical and have a radial anisotropic velocity dispersion ( $\overline{v_r^2} \neq \overline{v_\theta^2} = \overline{v_\phi^2}$ ). Called King-Michie models, they associate the lowered maxwellian of the King model with the anisotropy factor of the Eddington models:

$$f(\varepsilon, l) \propto (\exp(-2j^2\varepsilon) - \exp(-2j^2\varepsilon_t)) \exp(-j^2l^2/r_a^2) \quad (6)$$

Lupton & Gunn (1987) developed multi-mass models whose distribution functions depend on a third integral of motion  $I_3$ , in addition to the stellar energy per unit mass  $\varepsilon$  and the component of angular momentum parallel to the rotation axis  $l_z$ . Although no general analytical form for a third integral is available, the existence of an analytic third integral of motion  $I_3$  in special cases has been known for decades, since the work by Jeans (1915). Because the rotation creates a non-spherical potential,  $I_3 = l^2$  is in fact only an approximate integral and Lupton & Gunn's distribution function does not obey the collisionless Boltzmann's equation for equilibrium (Eq. 4).

These were notable landmarks in these developments, among many others. Table 2 hereafter, from Meylan & Heggie (1997), list for the static models (King, King-Michie, 3-Integral) and for the evolutionary models (gas, Fokker-Planck, N-Body) the dynamical features and dynamical processes they take into account. Under the heading Dynamical Process, the second column in Table 2 states what kind of physical process it is that is named in the first column.

#### 4 Parametric and non-parametric approaches

The method in the above section for analyzing globular cluster data is a model-building, or parametric, approach. One begins by postulating a functional form for the distribution function  $f$  and the gravitational potential  $\Phi$ ; often the two are linked via Poisson's equation, i.e. the stars described by  $f$  are assumed to contain all of the mass that contributes to  $\Phi$ . This  $f$  is then projected into observable space and its predictions compared with the data. If the discrepancies are significant, the model is rejected and another one is tried. If no combination of functions  $\{f, \Phi\}$  from the adopted family can be

Table 2. Dynamical models of globular star clusters

		Static Models			Evolutionary Models		
		King	Michie-King	3-Integral	Gas	Fokker-Planck	N-Body
Dynamical Features							
Anisotropy		...	✓	✓	✓	✓	✓
Rotation		...	...	✓	...	✓	✓
Flattening		...	...	✓	...	✓	✓
Dynamical Processes							
Stellar evolution	1-body	...	...	...	✓	✓	✓
Relaxation	2-body	✓	✓	✓	✓	✓	✓
Tidal Interactions	2-body	...	...	...	...	✓	✓
Collisions	2-body	✓	...	...	...	✓	✓
Stellar Escape	2-body	✓	...	...	...	✓	✓
Primordial Binaries	3- and 4-body	...	...	...	✓	✓	✓
Stellar Motions	collisionless	✓	✓	✓	✓	✓	✓
Steady Tide	collisionless	✓	✓	✓	...	✓	✓
Disk Shocking	collisionless	...	...	...	...	✓	✓

found that reproduces the data, one typically adds extra degrees of freedom until the fit is satisfactory. For instance,  $f$  may be allowed to depend on a larger number of integrals of the motion (Lupton & Gunn 1987) or the range of possible potentials may be increased by postulating additional populations of unseen stars (Da Costa & Freeman 1976).

This approach has enjoyed considerable popularity, in part because it is computationally straightforward but also because, as King (1981) has emphasized, globular cluster data are generally well fitted by these standard models. But one never knows which of the assumptions underlying the models are adhered to by the real system and which are not. For instance, a deviation between the surface density profile of a globular cluster and the profile predicted by an isotropic model is sometimes taken as evidence that the real cluster is anisotropic. But it is equally possible that the adopted form for  $f(\varepsilon)$  is simply in error, since by adjusting the dependence of  $f$  on  $\varepsilon$  one can reproduce any density profile without anisotropy. Even including the additional constraint of a measured velocity dispersion profile does not greatly improve matters since it is always possible to trade off the mass distribution with the velocity anisotropy in such a way as to leave the observed dispersions unchanged (Dejonghe & Merritt 1992). Conclusions drawn from the model-building studies are hence very difficult to interpret; they are valid only to the extent that the assumed functional forms for  $f$  and  $\Phi$  are correct.

These arguments suggest that it might be profitable to interpret kinematical data from globular clusters in an entirely different manner, placing much stronger demands on the data and making fewer ad hoc assumptions about  $f$  and  $\Phi$ . Ideally, the unknown functions should be generated non-parametrically from the data. Such an approach pioneered by Merritt (see, e.g., Merritt 1993a,b, 1996) has rarely been tried in the past because of the inherent instability of the deprojection process. We provide here after the results of two studies (parametric and non-parametric, respectively) of the globular cluster  $\omega$  Centauri, both studies using exactly the same observational data (surface brightness profile and stellar radial velocities).

#### 4.1 Parametric approach applied to $\omega$ Centauri

The mean radial velocities obtained with CORAVEL (Mayor et al. 1997) for 469 individual stars located in the galactic globular cluster  $\omega$  Centauri provide the velocity dispersion profile. It increases significantly from the outer parts inwards: the 16 outermost stars, located between  $19.2'$  and  $22.4'$  from the center, have a velocity dispersion  $\sigma = 5.1 \pm 1.6 \text{ km s}^{-1}$ , while the 16 innermost stars, located within  $1'$  from the center, have a velocity dispersion  $\sigma = 21.9 \pm 3.9 \text{ km s}^{-1}$ . This inner value of about  $\sigma_o = 22 \text{ km s}^{-1}$  is the largest velocity dispersion value obtained in the core of any galactic globular cluster (Meylan et al. 1995).

A simultaneous fit of these radial velocities and of the surface brightness profile to a multi-mass King-Michie dynamical model provides mean estimates



of the total mass equal to  $M_{tot} = 5.1 \cdot 10^6 M_{\odot}$ , with a corresponding mean mass-to-light ratio  $M/L_V = 4.1$ . The present results emphasize the fact that  $\omega$  Centauri is not only the brightest but also, by far, the most massive galactic globular cluster (Meylan et al. 1995).

The fact that only models with strong anisotropy of the velocity dispersion ( $r_a = 2-3 r_c$ ) agree with the observations does not give a definitive proof of the presence of such anisotropy because of fundamental indetermination in the comparison between King-Michie models and observations. A strong anisotropy is nevertheless expected outside of the core of  $\omega$  Centauri, given the large value of the half-mass relaxation time of about  $26 \leq t_{rh} \leq 46 \cdot 10^9 \text{yr}$  (Meylan et al. 1995).

The reliability of the present application of King-Michie models might be questionable on a few fundamental points. In addition to the arbitrary choices of the two integrals of the motion and of the functional dependence of the distribution function on these two integrals, there is also the assumption of thermal equilibrium among the different mass classes in the central parts of the cluster. From a theoretical point of view, mass segregation has been one of the early important results to emanate from small N-body simulations. Since then, large N-body simulations and models integrating the Fokker-Planck equation for many thousands of stars have fully confirmed the presence of equipartition. Thanks to the high angular resolution of the Hubble Space Telescope (HST) cameras (FOC and WFPC2), mass segregation has now been observed in the core of a few galactic globular clusters (see, e.g., Anderson 1997, 1999). In the case of 47 Tucanae, the observed luminosity function by Anderson (1997, 1999) is in close agreement with equipartition-assuming King-Michie models and fails to fit the no-segregation models. This dichotomy is not as clear in the case of  $\omega$  Centauri, probably because of its rather long central relaxation time.

The problem about mass segregation does not concern its existence — it is happening —, but rather its quantitative evolution. Can there be an end to mass segregation, i.e., does the system ever reach a stable thermal equilibrium? Underlying is the problem of core collapse (see Spitzer 1969, Chernoff & Weinberg 1990), which is briefly described in § 7 below.

#### 4.2 *Non-parametric approach applied to $\omega$ Centauri*

The stellar dynamics of  $\omega$  Centauri is inferred from the same radial velocities of 469 stars used in § 4.1 (Mayor et al. 1997). By assuming that the residual velocities are isotropic in the meridional plane,  $\sigma_{\varpi} = \sigma_z \equiv \sigma$ , Merritt et al. (1997) derived the dependence of the two independent velocity disper-

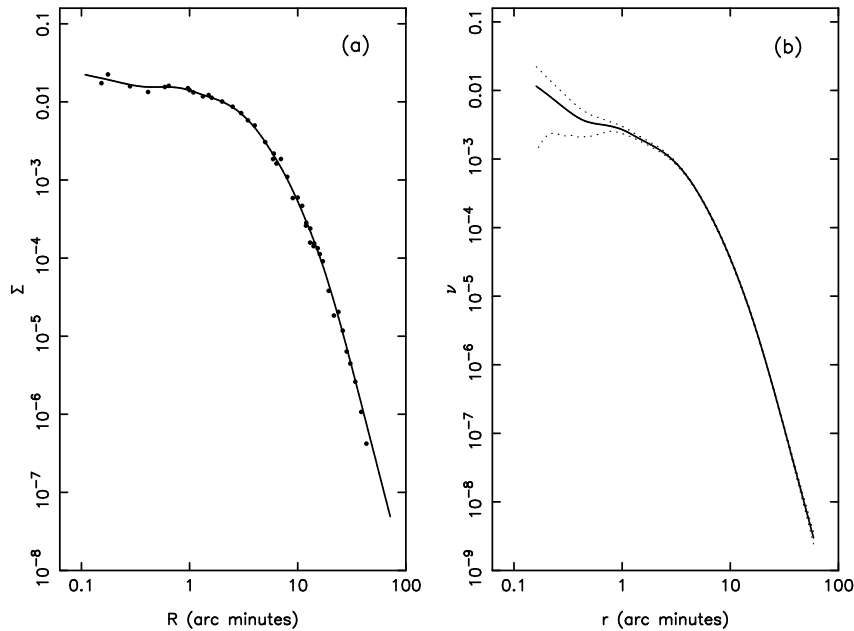


Figure 2. Surface brightness (a) and space density (b) profiles for  $\omega$  Centauri from Merritt et al. (1997).

sions  $\sigma$  and  $\sigma_\phi$  on various positions in the meridional plane. The central velocity dispersion parallel to the meridional plane is  $\sigma_o = 17_{-2.6}^{+2.1} \text{ km s}^{-1}$ . With this approach, there is no evidence for significant anisotropy anywhere in  $\omega$  Centauri. Thus, this cluster can reasonably be described as an isotropic oblate rotator (Merritt et al. 1997).

The binned surface brightness measurements from Meylan (1986) are plotted in Fig. 2a, where the solid line in is an estimate of the surface brightness profile  $\Sigma(R)$ , as the solution to the optimization problem. The estimate of space density profile  $\nu(r)$  may be defined as the Abel inversion of the estimate  $\Sigma(R)$ :

$$\nu(r) = -\frac{1}{\pi} \int_r^\infty \frac{d\Sigma}{dR} \frac{dR}{\sqrt{R^2 - r^2}}. \quad (7)$$

The dashed lines in Fig. 2b are 95% confidence bands on the estimate of  $\nu(r)$ . Here  $r$  is an azimuthally-averaged mean radius. Both profiles are normalized to unit total number. This profile actually has a power-law cusp,  $\nu \sim r^{-1}$ ,

inside of  $0.5'$ ; however the confidence bands are consistent with a wide range of slopes in this region, including even a profile that declines toward the center.

The gravitational potential and mass distribution in  $\omega$  Centauri are consistent with the predictions of a model in which the mass is distributed in the same way as the bright stars, although the cluster is assumed to be oblate and edge-on but mass is not assumed to follow light. The central mass density is  $2110_{-510}^{+530} M_{\odot} \text{pc}^{-3}$ . However this result may be strongly dependent on the assumption that the velocity ellipsoid is isotropic in the meridional plane. This central mass density determination is in full agreement with the values deduced from King-Michie models by Meylan et al. (1995).

There is no significant evidence for a difference between the velocity dispersions parallel and perpendicular to the meridional plane. The mass distribution inferred from the kinematics is slightly more extended than, though not strongly inconsistent with, the luminosity distribution. The derived two-integral distribution function  $f(\varepsilon, l_z)$  for the stars in  $\omega$  Centauri is fully consistent with the available data.

Large amount of kinematical data (radial velocities and proper motions for a few thousand stars) will soon allow the efficient use of the non-parametric approach in the case of the largest two galactic globular clusters, viz.  $\omega$  Centauri and 47 Tucanae (Freeman et al., Meylan et al., both in preparation).

## 5 Systemic rotation of $\omega$ Centauri

Systemic rotation in globular clusters has been expected for a long time, especially in  $\omega$  Centauri, because of its significant flattening. The first clear evidence of such rotation was observed, in this cluster and in 47 Tucanae, by Meylan & Mayor (1986). More recently, rather than fitting the data to a family of models, estimate of the rotation was obtain non-parametrically, by direct operation on the data by Merritt et al. (1997).

Fig. 3 displays the contours of constant  $\bar{v}_{\phi}$  which are remarkably similar in shape to those of the parametric model postulated by Meylan & Mayor (1986), at least in the region near the center where the solution is strongly constrained by the data. The rotational velocity field is clearly not cylindrical; instead,  $\bar{v}_{\phi}$  has a peak value of  $8 \text{ km s}^{-1}$  at about  $7'$  from the center in the equatorial plane, and falls off both with increasing  $\varpi$  and  $z$ . In the region inside the peak, the rotation is approximately solid-body; at large radii, the available data do not strongly constrain the form of the rotational velocity field. The mean motions are consistent with axisymmetry, once a correction is made for perspective rotation resulting from the cluster proper motion.

The above inferred rotational velocity field in  $\omega$  Centauri agree remark-

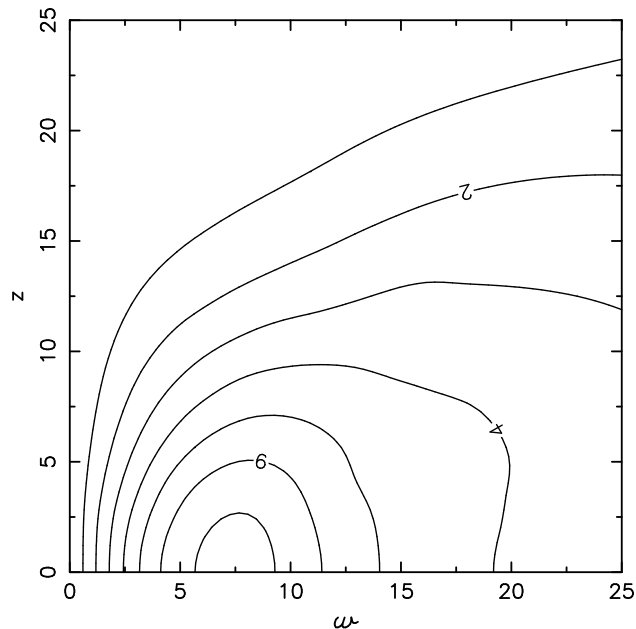


Figure 3. Rotation in NGC 5139  $\equiv$   $\omega$  Centauri: estimate of the mean azimuthal velocity  $\bar{v}_\phi$  in the meridional plane of  $\omega$  Centauri, displayed here in the North-West quadrant. Distances are in arc minutes and contours are labeled in  $\text{km s}^{-1}$ . From Merritt et al. (1997).

ably with the predictions of the theoretical model by Einsel & Spurzem (1999), who have investigated the influence of rotation on the dynamical evolution of collisional stellar systems by solving the orbit-averaged Fokker-Planck equation in  $(\varepsilon, l_z)$ -space. However it is not clear that any relevant comparison exists: because of the long relaxation time in  $\omega$  Centauri, the rotation probably still reflects to a large extent the state of the cluster shortly after its formation. The observed estimate of  $\bar{v}_\phi(\varpi, z)$  might therefore be most useful as a constraint on cluster formation models.

But things may be even more complicated ! Using their calcium abundances for about 400 stars with radial velocities by Mayor et al. (1997), Norris et al. (1997) found that the 20% metal-rich tail of the  $[\text{Ca}/\text{H}]$  distribution is not only more centrally concentrated, but is also kinematically cooler than the 80% metal-poor component. While the metal-poorer component exhibits well-defined systemic rotation, the metal-richer one shows no evidence of it, in contradistinction to the simple dissipative enrichment scenario of cluster

formation.

## 6 Rotation vs. velocity dispersion

All results about rotation depend on the value of the angle  $i$  between the plane of the sky and the axis of symmetry of the cluster. This angle remains unknown. Since the two best studied clusters, viz.  $\omega$  Centauri and 47 Tucanae, belong to the small group of clusters which, among the 150 galactic globular clusters, are the flattest ones, we can expect, from a statistical point of view, that their angles  $i$  should not be very different from  $0^\circ \leq i \leq 30^\circ$ , the clusters being seen nearly edge-on. The importance of rotation (namely, of its projection along the line of sight) increases as  $i$  gets closer to  $0^\circ$ .

The relative importance of rotational to random motions is given by the ratio  $v_o/\sigma_o$ , where  $v_o^2$  is the mass-weighted mean square rotation velocity and  $\sigma_o^2$  is the mass-weighted mean square random velocity. For  $i = 90^\circ$  and  $60^\circ$ , in  $\omega$  Centauri the ratio  $v_o/\sigma_o = 0.35$  and  $0.39$  and in 47 Tucanae the ratio  $v_o/\sigma_o = 0.40$  and  $0.46$ , respectively (Meylan & Mayor 1986). Even with  $i = 45^\circ$ , the dynamical importance of rotation remains weak compared to random motions. The ratio of rotational to random kinetic energies is  $\simeq 0.1$ , confirming the fact that globular clusters are, above all, hot stellar systems.

Rotation has been directly observed and measured in twelve globular clusters (see Table 7.2 in Meylan & Heggie 1997). The diagram ( $v_o/\sigma_o$  vs.  $\langle\varepsilon\rangle$ ), of the ratio of ordered  $v_o$  to random  $\sigma_o$  motions as a function of the ellipticity  $\langle\varepsilon\rangle$ , has been frequently used for elliptical galaxies and its meaning is extensively discussed in Binney & Tremaine (1987 Chapter 4.3). The low luminosity ( $L \lesssim 2.5 \cdot 10^{10} L_\odot$ ) elliptical galaxies and spheroids have ( $v_o/\sigma_o, \langle\varepsilon\rangle$ ) values which are scattered along the relation for oblate systems with isotropic velocity-dispersion tensors, while the high luminosity ( $L \gtrsim 2.5 \cdot 10^{10} L_\odot$ ) elliptical galaxies have ( $v_o/\sigma_o, \langle\varepsilon\rangle$ ) values which are scattered below the above relation, indicating the presence of anisotropic velocity-dispersion tensors. Given their small mean ellipticities ( $0.00 \leq \langle\varepsilon\rangle \leq 0.12$ ), globular clusters are located in the lower-left corner of the ( $v_o/\sigma_o$  vs.  $\langle\varepsilon\rangle$ ) diagram, an area characterized by isotropy or mild anisotropy of the velocity-dispersion tensor.

## 7 Overwhole dynamical evolution towards core collapse

Till the late ninety seventies, globular clusters were thought to be relatively static stellar systems since most surface-brightness profiles of globular clusters were successfully fitted by equilibrium models. Nevertheless, it had been already known, since the early sixties, that globular clusters had to evolve

dynamically, even when considering only relaxation, which causes stars to escape, consequently cluster cores to contract and envelopes to expand. But dynamical evolution of globular clusters was not yet a field of research by itself, since the very few theoretical investigations had led to a most puzzling paradox: core collapse (Hénon 1961, Lynden-Bell & Wood 1968).

It was only in the early eighties that the field grew dramatically. On the theoretical side, the development of high-speed computers allowed numerical simulations of dynamical evolution. Nowadays, Fokker-Planck and conducting-gas-sphere evolutionary models have been computed well into core collapse and beyond, leading to the discovery of possible post-collapse oscillations. In a similar way, hardware and software improvements of N-body codes provide very interesting first results for  $10^4$ -body simulations (Makino 1996a,b, Spurzem & Aarseth 1996, Portegies Zwart et al. 1999), and give the first genuine hope, in a few years, for  $10^5$ -body simulations. On the observational side, the manufacture of low-readout-noise Charge Coupled Devices (CCDs), combined since 1990 with the high spatial resolution of the Hubble Space Telescope (HST), allow long integrations on faint astronomical targets in crowded fields, and provide improved data analyzed with sophisticated software packages.

## 8 Gravothermal instability, gravothermal oscillations

For many years (between about 1940 and 1960) secular evolution of globular cluster was understood in terms of the evaporative model of Ambartsumian (1938) and Spitzer (1940). In this model it is assumed that two-body relaxation attempts to set up a maxwellian distribution of velocities on the time scale of a relaxation time, but that stars with velocities above the escape velocity promptly escape. The next major step in understanding came when it was discovered that evolution arises also when stars escape from the inner parts of the cluster to larger radii, without necessarily escaping altogether. Antonov (1962) realised that these internal readjustments need not lead to a structure in thermal equilibrium, because thermal equilibrium may be unstable in self-gravitating systems (see Lynden-Bell & Wood 1968). The well known process of core collapse is interpreted as a manifestation of the gravothermal instability.

Core collapse has been first observed and studied in simulations using gas and Fokker-Planck models. For an isolated cluster (without a tidal field) the time scale for the entire evolution of the core (when the density has formally become infinite) is about  $15.7 t_{rh}(0)$ , when expressed in terms of the initial half-mass relaxation time (Cohn 1980). This result is for an isotropic

code starting from a Plummer model with stars of equal mass, while for an anisotropic code the time extends to  $17.6 t_{rh}(0)$  (Takahashi 1995).

The collapse time is generally shorter in the presence of unequal masses (Inagaki & Wiyanto 1984, Chernoff & Weinberg 1990). Murphy & Cohn (1988) give surface brightness and velocity dispersion profiles at various times during collapse, for a system with a reasonably realistic present-day mass spectrum. Addition of effects of stellar evolution, modeled as instantaneous mass loss at the end of main sequence evolution, delays the onset of core collapse (Angeletti & Giannone 1980, Applegate 1986, Chernoff & Weinberg 1990, Kim et al. 1992). The effect of a galactic time-dependent tidal field can be to accelerate core collapse (Spitzer & Chevalier 1973).

Examples of  $N$ -body models which illustrate various aspects of core collapse include Aarseth (1988), where  $N = 1,000$ , Giersz & Heggie (1993) ( $N \leq 2,000$ ), Spurzem & Aarseth (1996) ( $N = 10,000$ ), and Makino (1996a,b; see Fig. 4 hereafter) ( $N \leq 32,000$ ).

At one time, it was not at all certain that a cluster could survive beyond the end of core collapse, with as a singularity characterized by infinite central density. Thus, many experts doubted whether the study of post-collapse clusters had any relevance to the interpretation of observations. Hénon (1961, 1965) showed that a cluster without such a singularity would evolve into one that did, and he realised that, in a real system, a flux of energy might well be supplied by the formation and evolution of binary stars, governing a series of collapses and expansions of the cluster core.

Numerical simulations using gas and Fokker-Planck models show that systems with at least a few thousand stars (Goodman 1987, Heggie & Ramamani 1989, Breeden et al. 1994) follow a complicated succession of collapses and expansions, called gravothermal oscillations by their discoverers (Sugimoto & Bettwieser 1983, Bettwieser & Sugimoto 1984). Quite apart from their relevance in nature, these oscillations are interesting in their own right, as an example of chaotic dynamics. From this point of view they have been studied by Allen & Heggie (1992), Breeden & Packard (1994), and Breeden & Cohn (1995).

In 1995 the genuine occurrence of gravothermal oscillations in  $N$ -body systems was spectacularly demonstrated by Makino (1996a,b). These results confirm that the nature of post-collapse evolution in  $N$ -body systems is far more stochastic than in the simplified continuum models on which so much of our understanding rests at present.

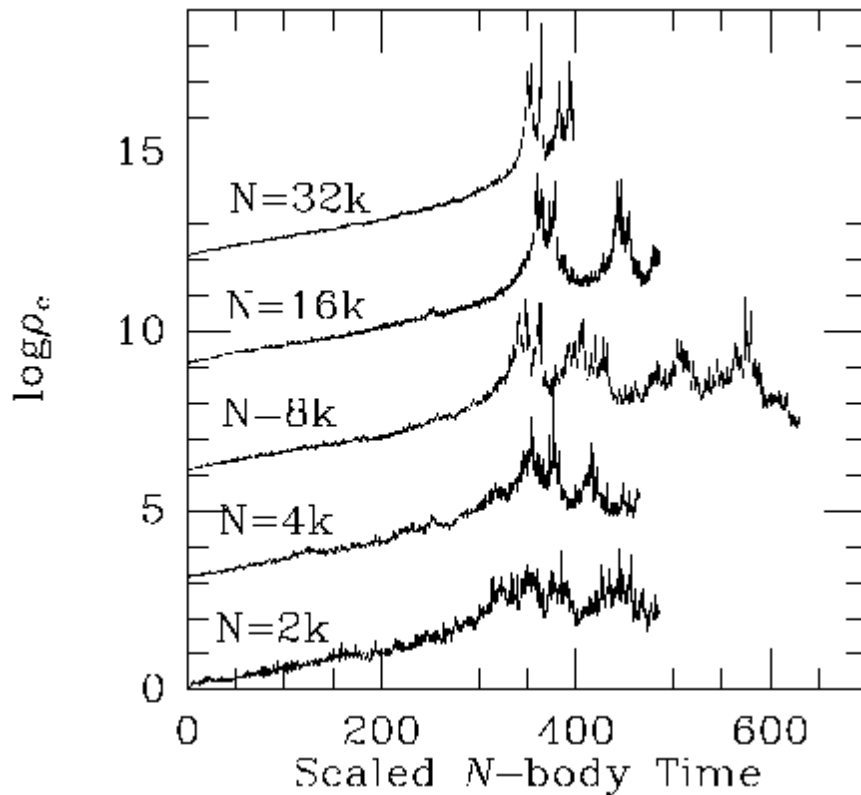


Figure 4. Core collapse in systems with equal masses, from  $N$ -body integrations by Makino (1996b). The logarithm of the central density is plotted against time, scaled in proportion to the initial half-mass relaxation time. The successive curves, which correspond to different values of  $N$ , have been displaced vertically for clarity. For  $N \leq 32,000$  the first core collapse is clearly followed by gravothermal oscillations.

## 9 Observational evidence of core collapse

In the eighties, CCD observations allowed a systematic investigation of the inner surface brightness profiles (within  $\sim 3'$ ) of 127 galactic globular clusters (Djorgovski & King 1986, Chernoff & Djorgovski 1989, Trager et al. 1995). These authors sorted the globular clusters into two different classes: (i) the King model clusters, whose surface brightness profiles resemble a single-component King model with a flat isothermal core and a steep envelope, and



(ii) the collapsed-core clusters, whose surface brightness profiles follow an almost pure power law with an exponent of about  $-1$ . In the Galaxy, about 20% of the globular clusters belong to the second type, exhibiting in their inner regions apparent departures from King-model profiles. Consequently, they are considered to have collapsed cores.

The globular cluster M15 has long been considered as a prototype of the collapsed-core star clusters. High-resolution imaging of the centre of M15 has resolved the luminosity cusp into essentially three bright stars. Post-refurbishment HST star-count data confirm that the  $2.2''$  core radius observed by Lauer et al. (1991), and questioned by Yanny et al. (1994), is observed neither by Guhathakurta et al. (1996) with WFPC2 data nor by Sosin & King (1996) with FOC data. This surface-density profile clearly continues to climb steadily within  $2''$ . A maximum-likelihood method rules out a  $2''$  core at the 95% confidence level. It is not possible to distinguish at present between a pure power-law profile and a very small core (Sosin & King 1996). Consequently, among the galactic globular clusters, M15 displays one of the best cases of clusters caught in a state of deep core collapse.

## 10 Tidal tails from wide-field imaging

### 10.1 Tidal truncation

In addition to the effects of their internal dynamical evolution, globular clusters suffer strong dynamical evolution from the potential well of their host galaxy (Gnedin & Ostriker 1997, Murali & Weinberg 1997). These external forces speed up the internal dynamical evolution of these stellar systems, accelerating their destruction. Shocks are caused by the tidal field of the galaxy: interactions with the disk, the bulge and, somehow, with the giant molecular clouds, heat up the outer regions of each star cluster. The stars in the halo are stripped by the tidal field. All globular clusters are expected to have already lost an important fraction of their mass, deposited in the form of individual stars in the halo of the Galaxy (see Meylan & Heggie 1997 for a review).

Recent N-body simulations of globular clusters embedded in a realistic galactic potential (Oh & Lin 1992; Johnston et al. 1999) were performed in order to study the amount of mass loss for different kinds of orbits and different kinds of clusters, along with the dynamics and the mass segregation in tidal tails. Grillmair et al. (1995) in an observational analysis of star counts in the outer parts of a few galactic globular clusters found extra-cluster overdensities that they associated partly with stars stripped into the Galaxy field.

### 10.2 *Tidal tails from wide-field observations*

Leon, Meylan & Combes (2000) studied the 2-D structures of the tidal tails associated with 20 galactic globular clusters, obtained by using the wavelet transform to detect weak structures at large scale and filter the strong background noise for the low galactic latitude clusters. They also present N-body simulations of globular clusters in orbits around the Galaxy, in order to study quantitatively and geometrically the tidal effects they encounter (Combes, Leon & Meylan 2000).

Their sample clusters share different properties or locations in the Galaxy, with various masses and structural parameters. It is of course necessary to have very wide field imaging observations. Consequently, they obtained, during the years 1996 and 1997, photographic films with the ESO Schmidt telescope. The field of view is  $5.5^\circ \times 5.5^\circ$  with a scale of  $67.5''/\text{mm}$ . The filters used, viz. BG12 and RG630, correspond to  $B$  and  $R$ , respectively. All these photographic films were digitalized using the MAMA scanning machine of the Observatoire de Paris, which provides a pixel size of  $10 \mu\text{m}$ . The astrometric performances of the machine are described in Berger et al. (1991).

The next step — identification of all point sources in these frames — was performed using SExtractor (Bertin & Arnouts 1996), a software dedicated to the automatic analysis of astronomical images using a multi-threshold algorithm allowing good object deblending. The detection of the stars was done at a  $3\text{-}\sigma$  level above the background. This software, which can deal with huge amounts of data (up to  $60,000 \times 60,000$  pixels) is not suited for very crowded fields like the centers of the globular clusters, which were simply ignored. A star/galaxy separation was performed by using the method of star/galaxy magnitude vs.  $\log(\text{star/galaxy area})$ .

For each field, a ( $B$  vs.  $B - V$ ) color-magnitude diagram was constructed, on which a field/cluster star selection was performed, following the method of Grillmair et al. (1995), since cluster stars and field stars exhibit different colors. In this way present and past cluster members could be distinguished from the fore- and background field stars by identifying in the CMD the area occupied primarily by cluster stars. The envelope of this area is empirically chosen so as to optimize the ratio of cluster stars to field stars in the relatively sparsely populated outer regions of each cluster.

### 10.3 *Wavelet Analysis*

With the assumption that the data can be viewed as a sum of details with different typical scale lengths, the next step consists of disentangling these details using the space-scale analysis provided by the Wavelet Transform (WT,

cf. Slezak et al. 1994; Resnikoff & Wells 1998). Any observational signal includes also some noise, which has a short scale length. Consequently the noise is higher for the small scale wavelet coefficients. Monte-Carlo simulations were performed to estimate the noise at each scale and apply a  $3\text{-}\sigma$  threshold on the wavelet coefficients to keep only the reliable structures. In this way it is possible to subtract the short-wavelength noise without removing details from the signal which has longer wavelengths. The remaining overdensities of the cluster-like stars, remaining after the application of the wavelength transform analysis to the star counts, are associated with the stars evaporated from the clusters because of dynamical relaxation and/or tidal stripping by the galactic gravitational field.

It is worth emphasizing that in this study, the following strong observational biases were taken into account: (i) bias due to the clustering of galactic field stars; (ii) bias due to the clustering of background galaxies; (iii) bias due to the fluctuations of the dust extinction, as observed in the IRAS  $100\text{-}\mu\text{m}$  map.

#### 10.4 *Observational Results*

The most massive galactic globular cluster,  $\omega$  Centauri (Meylan et al. 1995), currently crossing the disk plane, is a nearby globular cluster located at a distance of 5.0 kpc from the sun. Its relative proximity allows, for the star count selection, to reach the main sequence significantly below the turn-off. Estimates, taking into account the possible presence of mass segregation in its outer parts, show that about 0.6 to 1 % of its mass has been lost during the current disk shocking event. Although this cluster has, in this study, one of the best tail/background S/N ratios, it is by far not the only one exhibiting tidal tails.

Considering all 20 clusters of the sample, the following conclusions are reached (see Leon, Meylan & Combes 2000 for a complete description of this work):

- All the clusters observed, which do not suffer from strong observational biases, present tidal tails, tracing their dynamical evolution in the Galaxy (evaporation, tidal shocking, tidal torquing, and bulge shocking).
- The clusters in the following sub-sample (viz. NGC 104, NGC 288, NGC 2298, NGC 5139, NGC 5904, NGC 6535, and NGC 6809) exhibit tidal extensions resulting from a recent shock, i.e. tails aligned with the tidal field gradient.
- The clusters in another sub-sample (viz. NGC 1261, NGC 1851,

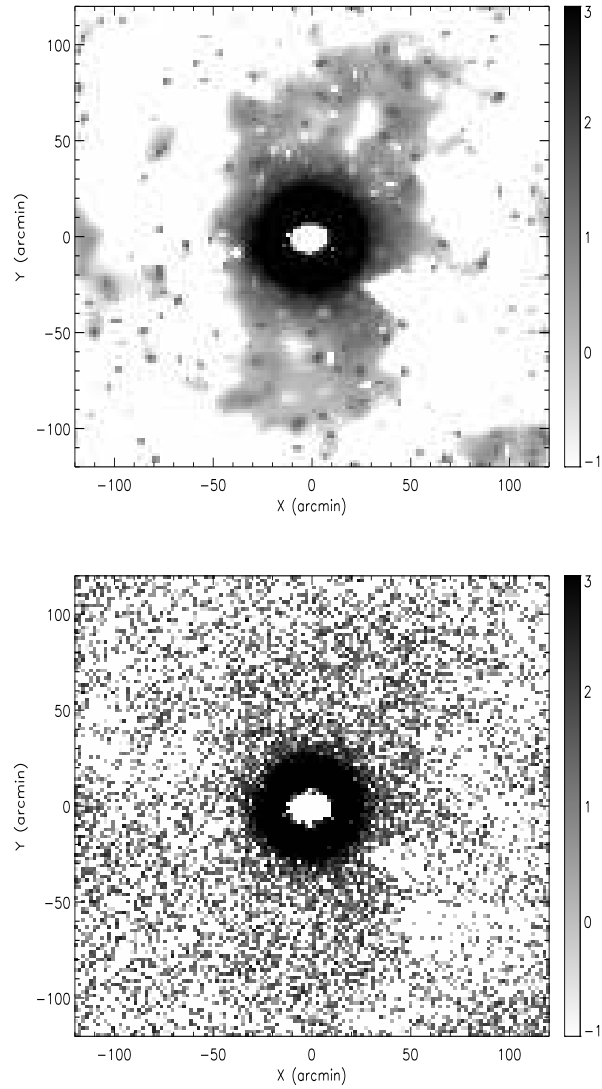


Figure 5. NGC 5139  $\equiv \omega$  Centauri. In the upper panel, filtered image of color-selected star-count overdensities using the Wavelet Transform to be compared with the raw star counts in the lower panel. The upper panel displays the full resolution using the whole set of wavelet planes. From Leon et al. (2000).

NGC 1904, NGC 5694, NGC 5824, NGC 6205, NGC 7492, Pal 5, and Pal 12) present extensions which are only tracing the orbital path of the cluster with various degrees of mass loss.

- NGC 7492 is a striking case because of its very small extension and its high destruction rate driven by the galaxy as computed by Gnedin & Ostriker (1997). Its dynamical twin for such an evolution, namely Pal 12, exhibits, on the contrary, a large extension tracing its orbital path, with a possible shock which happened more than 350 Myr ago.
- The presence of a break in the outer surface density profile is a reliable indicator of some recent gravitational shocks.

Recent CCD observations with the Wide Field Imager at the ESO/MPI 2.2-m telescope and with the CFH12K camera at the Canada-France-Hawaii 3.6-m telescope will soon provide improved results, because of the more accurate CCD photometry. These observations will allow more precise observational estimates of the mass loss rates for different regimes of galaxy-driven cluster evolution.

### 10.5 Numerical Simulations

Extensive numerical N-body simulations of globular clusters in orbit around the Galaxy were performed in order to study quantitatively and geometrically the tidal effects they encounter and to try to reproduce the above observations. The N-body code used is an FFT algorithm, using the method of James (1977) to avoid the periodic images. With  $N = 150,000$  particles, it required 2.7 seconds of CPU per time step on a Cray-C94.

The globular clusters are represented by multi-mass King-Michie models, including mass segregation at initial conditions. The Galaxy is modeled as realistically as possible, with three components, bulge, disk and dark halo: the bulge is a spherical Plummer law, the disk is a Miyamoto-Nagai model, and the dark matter halo is added to obtain a flat galactic rotation curve.

The main conclusions of these simulations can be summarized as follows (see Combes, Leon & Meylan 2000 for a complete description of this work):

- All runs show that the clusters are always surrounded by tidal tails and debris. This is also true for those that suffered only a very slight mass loss. These unbound particles distribute in volumic density like a power-law as a function of radius, with a slope around  $-4$ . This slope is much steeper than in the observations where the background-foreground contamination dominates at very large scale.

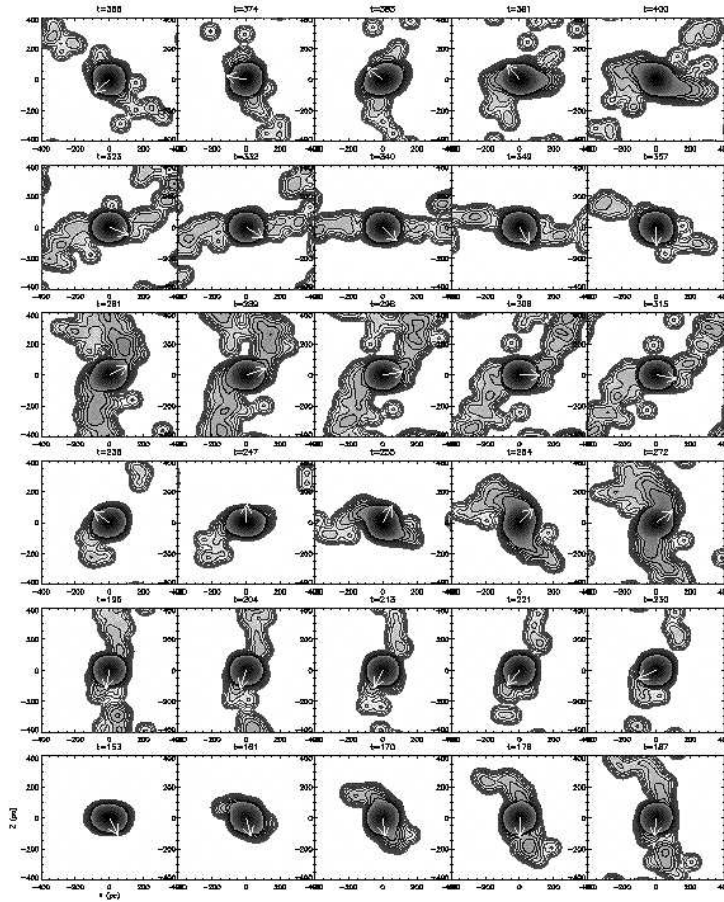


Figure 6. Tidal tails mapped at different epochs with the wavelet algorithm applied to one of our simulations. The direction perpendicular to the galactic plane is indicated by the arrow. The time sequence starts with the lower-left panel and ends with the upper right one. The third panel exhibits tails which are quite reminiscent of what is observed in NGC 5139  $\equiv$   $\omega$  Centauri (see Fig. 5 above). From Combes et al. (2000).

- These tails are preferentially composed of low mass stars, since they are coming from the external radii of the cluster; due to mass segregation built up by two-body relaxation, the external radii preferentially gather the low mass stars.

- For sufficiently high and rapid mass loss, the cluster takes a prolate shape, whose major axis precesses around the z-axis.
- When the tidal tail is very long (high mass loss) it follows the cluster orbit: the observation of the tail geometry is thus a way to deduce cluster orbits. Stars are not distributed homogeneously through the tails, but form clumps, and the densest of them, located symmetrically in the tails, are the tracers of the strongest gravitational shocks.

Finally, these N-body experiments help to understand the recent observations of extended tidal tails around globular clusters (Grillmair et al. 1995, Leon et al. 2000): the systematic observations of the geometry of these tails should provide much information on the orbit, dynamics, and mass loss history of the clusters, and on the galactic structure as well.

## 11 G1 in M31: globular cluster or dwarf galaxy ?

The globular cluster Mayall II  $\equiv$  G1, recently observed with the Hubble Space Telescope (HST) camera WFPC2 (Rich et al. 1996, Jablonka et al. 1999, 2000, Meylan et al. 2000), is a bright star cluster which belongs to our companion galaxy, Andromeda  $\equiv$  M31. Its integrated visual magnitude  $V = 13.75$  mag corresponds to an absolute visual magnitude  $M_V = -10.86$  mag, with  $E(B-V) = 0.06$  and a distance modulus  $(m - M)_{M31} = 24.43$  mag, implying a total luminosity of about  $L_V \sim 2 \times 10^6 L_\odot$ .

The coordinates of G1, viz.  $\alpha_{G1}(J2000.00) = 00^\circ 32' 46.878''$  and  $\delta_{G1}(J2000.00) = +39^\circ 34' 41.65''$ , when compared to the coordinates of the center of M31, viz.  $\alpha_{M31}(J2000.00) = 00^\circ 42' 44.541''$  and  $\delta_{M31}(J2000.00) = +41^\circ 16' 28.77''$ , place it at a projected distance of about  $3^\circ$ , i.e. 39.5 kpc from the center of M31. In spite of this rather large projected distance, both color-magnitude diagrams and radial velocities of G1 and M31, viz.  $V_r(G1) = -331 \pm 24 \text{ km s}^{-1}$  while  $V_r(M31) = -300 \pm 4 \text{ km s}^{-1}$  (21-cm HI line) and  $V_r(M31) = -295 \pm 7 \text{ km s}^{-1}$  (optical lines), completely support the idea that this cluster belongs to the globular cluster system of M31.

Our ( $V$  vs.  $V-I$ ) color-magnitude diagram reaches stars with magnitudes fainter than  $V = 27$  mag, with a well populated red horizontal branch at about  $V = 25.25$  mag; we confirm the existence of a blueward extension of the red horizontal branch clump as already observed by Rich et al. (1996). From model fitting, we determine a rather high mean metallicity of  $[\text{Fe}/\text{H}] = -0.95 \pm 0.09$ , somewhat between the previous determinations of  $[\text{Fe}/\text{H}] = -0.7$  (Rich et al. 1996) and  $[\text{Fe}/\text{H}] = -1.2$  (Bonoli 1987; Brodie & Huchra 1990).

From artificial star experiments, in order to estimate our true measurement errors, we observe a clear spread in our photometry that we attribute to an intrinsic metallicity dispersion among the stars of G1. Namely, adopting  $E(V - I) = 0.10$  implies a 1- $\sigma$  [Fe/H] dispersion of  $\pm 0.50$  dex; adopting  $E(V - I) = 0.05$  implies a 1- $\sigma$  [Fe/H] dispersion of  $\pm 0.39$  dex. In all cases, the intrinsic metallicity dispersion is significant and may be the consequence of self enrichment during the early stellar/dynamical evolution phases of this cluster.

We have at our disposal two essential observational constraints allowing the mass determination of Mayall II  $\equiv$  G1:

(i) First, its surface brightness profile from HST/WFPC2 images, providing essential structural parameters: the core radius  $r_c = 0.14'' = 0.52$  pc, the half-mass radius  $r_h = 3.7'' = 14$  pc, the tidal radius  $r_t \simeq 54'' = 200$  pc, implying a concentration  $c = \log(r_t/r_c) \simeq 2.5$  (Meylan et al. 2000).

(ii) Second, its central velocity dispersion from KECK/HIRES spectra, providing an observed velocity dispersion  $\sigma_{obs} = 25.1$  km s $^{-1}$ , and an aperture-corrected central velocity dispersion  $\sigma_o = 27.8$  km s $^{-1}$ .

### 11.1 King model and Virial mass estimates

We can first obtain simple mass estimates from King models and from the Virial (see, e.g., Illingworth 1976). The first estimate, King mass, is given by the simple equation:

$$\text{King mass} = \rho_c r_c^3 \mu = 167 r_c \mu \sigma_o^2 \quad (8)$$

where the core radius  $r_c = 0.52$  pc, the dimensionless quantity  $\mu = 220$  for  $c = \log(r_t/r_c) = 2.5$  (King 1966), and the central velocity dispersion  $\sigma_o = 27.8$  km s $^{-1}$ . These values determine a total mass for the cluster of  $M_{tot} = 15 \times 10^6 M_\odot$  with the corresponding  $M/L_V \simeq 7.5$ .

The second estimate, Virial mass, is given by the simple equation:

$$\text{Virial mass} = 670 r_h \sigma_o^2 \quad (9)$$

where the half-mass radius  $r_h = 14$  pc and central velocity dispersion  $\sigma_o = 27.8$  km s $^{-1}$ . These values determine a total mass for the cluster of  $M_{tot} = 7.3 \times 10^6 M_\odot$  with the corresponding  $M/L_V \simeq 3.6$ .

### 11.2 King-Michie model mass estimate

The existing observational constraints allow the use of a multi-mass King-Michie model as defined by Equ. 6 above. See §4.1 above and Meylan et al. (1995) in the case of such a model applied to  $\omega$  Centauri. In the case of



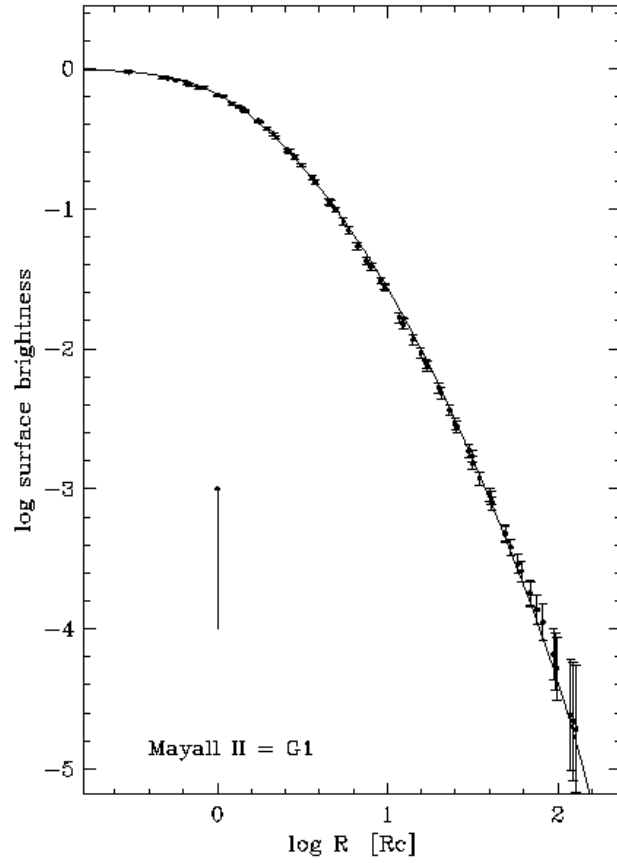


Figure 7. Surface brightness profile of the globular cluster Mayall II  $\equiv$  G1, from HST/WFPC2 shallow and deep images in F555W  $\simeq$  V filter; the continuous line represents a King-Michie model (first model in Table 3) fitted to the observed profile (Meylan et al. 2000).

Table 3. Multi-mass King-Michie models for Mayal II  $\equiv$  G1

$x_{MS}^{up}$	$x_{MS}^{down}$	$M_{hr+wd}$ %	conc $\log (r_t/r_c)$	$M_{tot}$ [ $10^6 M_\odot$ ]	$M/L_V$
1.35	-0.5	22	2.44	13.1	6.4
1.40	-0.2	21	2.49	13.9	6.8
1.40	+0.1	20	2.54	14.7	7.2
1.45	-0.3	20	2.48	14.0	6.9
1.45	+0.3	19	2.59	15.5	7.6
1.50	-0.4	20	2.48	14.1	7.0
1.50	+0.5	18	2.65	16.6	8.1
1.55	-0.5	20	2.47	14.1	7.0
1.55	+0.4	17	2.65	16.7	8.1
1.60	-0.3	19	2.53	15.0	7.4
1.60	+0.8	16	2.63	18.0	8.9

G1, such a model is simultaneously fitted to the surface brightness profile from HST/WFPC2 and to the central velocity dispersion value from KECK/HIRES.

An extensive grid of about 150,000 models was computed in order to explore the parameter space defined by the Initial Mass Function (IMF) exponent  $x$ , where  $x$  would equal 1.35 in the case of Salpeter (1955), the central gravitational potential  $W_\odot$ , and the anisotropy radius  $r_a$ . The IMF exponent consists actually of three parameters,  $x_{hr}$ , describing the heavy remnants, resulting from the already evolved stars with initial masses in the range between 0.85 and  $100 M_\odot$ ;  $x_{MS}^{up}$ , describing the stars still on the Main Sequence, with initial masses in the range between 0.25 and  $0.85 M_\odot$ ; and  $x_{MS}^{down}$  describing the stars still on the Main Sequence, with initial masses in the range between 0.10 and  $0.25 M_\odot$ .

Table 3 presents eleven of the 50 models with the lowest  $\chi^2$ , illustrating

some of the input and output parameters. Good models are considered as such not only on the basis of the  $\chi^2$  of the surface brightness fit (see Fig. 7), but also from their predictions of the observed integrated luminosity of the cluster and of the input mass-to-light ratio of the model. The different columns in Table 3 give, for each model, its IMF exponents  $x_{MS}^{up}$  and  $x_{MS}^{down}$ ; the fraction  $M_{hr}$  of its total mass in the form of heavy stellar remnants such as neutron stars and white dwarfs; its concentration  $c = \log(r_t/r_c)$ ; its total mass  $M_{tot}$  of the cluster, in solar units; and its corresponding mass-to-light ratio  $M/L_V$  also in solar units. Since the velocity dispersion profile is reduced to one single value — the central velocity dispersion — the models are not strongly constrained, providing equally good fits to rather different sets of parameters.

The IMF exponent  $x_{hr}$ , describing the amount of neutron stars, appears in all models to be very close to  $x = 1.35$  (Salpeter 1955). Given the lack of constraint from the absence of any velocity dispersion profile, the most reliable results are related to the concentration and the total mass. With a concentration  $c = \log(r_t/r_c)$  somewhere between 2.45 and 2.65, G1 presents clearly and in all cases the characteristics of a collapsed cluster. This is completely different from  $\omega$  Centauri, the most massive but loose galactic globular cluster, which, with a concentration of about 1.3, has a very large core radius of about 5 pc and is consequently very far from core collapse. With a total mass somewhere between 13 and 18  $10^6 M_\odot$ , and with the corresponding mass-to-light ratio  $M/L_V$  between 6 and 9, G1 is significantly more massive than  $\omega$  Centauri, maybe by up to a factor of three. The King-Michie mass estimates are in full agreement with the King mass estimate, while the Virial mass estimate is smaller by about a factor of two. It is worth mentioning that such a mass difference is not typical of G1: the same factor of about two is also observed between the King-Michie and Virial mass estimates of any cluster. See, e.g., Meylan & Mayor (1986) and Meylan et al. (1995) in the case of  $\omega$  Centauri.

### 11.3 *Mayall II $\equiv$ G1 is a genuine globular cluster*

From these three various mass determinations (King, Virial, King-Michie), we can reach the following conclusions about Mayall II  $\equiv$  G1:

- (i) All mass estimates give a total mass up to three times as large as the total mass of  $\omega$  Centauri;
- (ii) With  $c = \log(r_t/r_c) \simeq 2.5$ , G1 is more concentrated than 47 Tucanae, which is a massive galactic globular cluster considered on the verge of collapsing; G1 has a surface brightness profile typical of a collapsed cluster;
- (iii) G1 is the heaviest of the weighted globular clusters.

Given these results we can wonder if, even more than  $\omega$  Centauri, G1 could be a kind of transition step between globular clusters and dwarf elliptical galaxies. There is a way of checking this hypothesis. Kormendy (1985) used the four following quantities — the central surface brightness  $\mu_o$ , the central velocity dispersion  $\sigma_o$ , the core radius  $r_c$ , and the total absolute magnitude  $M$  — in order to define various planes from combinations of two of the above four quantities, e.g., ( $\mu_o$  vs.  $\log r_c$ ). In all these planes, the various stellar systems plotted by Kormendy (1985) segregate into three well separated sequences: (i) ellipticals and bulges, (ii) dwarf ellipticals, and (iii) globular clusters. When plotted on any of these planes, G1 appears always on the sequence of globular clusters, and cannot be confused or assimilated with either ellipticals and bulges or dwarf ellipticals. The same is true for  $\omega$  Centauri.

Consequently, Mayall II  $\equiv$  G1 can be considered a genuine bright and massive globular cluster. Actually, G1 may not be the only such massive globular cluster in M31. This galaxy, which has about twice as many globular clusters as our Galaxy, has at least three other clusters with central velocity dispersion larger than  $20 \text{ km s}^{-1}$  (Djorgovski et al. 1997). Unfortunately, so far, G1 is the only such cluster imaged with the high spatial resolution of the HST/WFPC2 camera, and consequently the only such massive cluster with known structural parameters. G1 and the other three bright M31 globular clusters represent probably the high-mass and high-luminosity tails of the otherwise very normal mass and luminosity distributions of the rich M31 population of globular clusters.

## 12 Conclusion

This review summarizes only parts of the tremendous developments that have taken place during the last two decades. These recent developments are far from having exploited all the new capabilities offered by the impressive progress in computer simulations, made possible by more powerful single-purpose hardware and software (Hut & Makino 1999, Spurzem 1998).

Observations too have still a lot of information to provide, which will require more elaborate modeling before full interpretation is reached. The mere observation of globular cluster stellar populations presents some puzzles which are far from being understood (Anderson 1997, 1999).

The kinematical and dynamical understanding of globular clusters will need the exploitation of numerous radial velocities and proper motions of individual stars. Only small quantities of radial velocities have been painfully accumulated over the last two decades, while the proper motions have so far simply been ignored. But there is an enormous amount of untapped infor-

mation locked in the radial velocities (for one third) and proper motions (for two thirds). Fortunately, a large amount of kinematical data (radial velocities and proper motions for a few thousand stars) will soon permit investigation of the 3-D space velocity distribution and rotation in the two largest galactic globular clusters, viz.  $\omega$  Centauri and 47 Tucanae (Freeman et al., Meylan et al., both in preparation).

### Acknowledgments

It is a pleasure to thank my following collaborators – T. Bridges (AAO), F. Combes (Paris), G. Djorgovski (Caltech), P. Jablonka (Paris), S. Leon (Paris), and A. Sarajedini (Wesleyan), – for allowing me to present some of our results in advance of publication.

### References

1. Aarseth S.J., 1988, Bol. Acad. Nac. Cienc. Cordoba, 58, 189
2. Allen F.S., Heggie D.C., 1992, MNRAS, 257, 245
3. Ambartsumian V.A., 1938, Ann. Leningrad State Univ., 22, 19; English translation: Ambartsumian V.A., 1985, in Dynamics of Star Clusters, IAU Symp. 113, eds. Goodman J. & Hut P., (Dordrecht: Reidel), p. 521
4. Anderson J., 1999, in preparation (see also Ph.D. thesis, 1997, University of California, Berkeley)
5. Angeletti L., Giannone P., 1980, A&A, 85, 113
6. Antonov V.A., 1962, Vest. leningr. gos. Univ., 7, 135; English translation: Antonov, V.A., 1985, in Dynamics of Star Clusters, IAU Symp. 113, eds. Goodman J. & Hut P., (Dordrecht: Reidel), p. 525
7. Applegate J.H., 1986, ApJ, 301, 132
8. Berger J., Cordoni J.P., Fringant A.M., Guibert J., Moreau, O., Reboul H., Vanderriest C., 1991, A&AS, 87, 389
9. Bertin E., Arnouts S., 1996, A&AS, 117, 393
10. Bettwieser E., Sugimoto D., 1984, MNRAS, 208, 493
11. Binney J., 1982, in Morphology and Dynamics of Galaxies, Saas-Fee Advanced Course 12, eds. Martinet L. & Mayor M., (Geneva: Geneva Observatory), p. 1
12. Binney J., Tremaine S., 1987, Galactic Dynamics, (Princeton: Princeton University Press)
13. Bonoli F., Delpino F., Federici L., Fusi Pecci F., 1987, A&A, 185, 25
14. Breeden J.L., Cohn H.N., Hut P., 1994, ApJ, 421, 195
15. Breeden J.L., Cohn H.N., 1995, ApJ, 448, 672

16. Breeden J.L., Packard N.H., 1994, *Int. J. Bifurcations and Chaos*, 4, 311
17. Brodie J.P., Huchra J.P., 1990, *ApJ*, 362, 503
18. Chernoff D.F., Djorgovski S.G., 1989, *ApJ*, 339, L904
19. Chernoff D.F., Weinberg M.D., 1990, *ApJ*, 351, 121
20. Cohn H., 1980, *ApJ*, 242, 765
21. Combes F., Leon S., Meylan G., 2000, *A&A*, in press
22. Da Costa G.S., Freeman K.C., 1976, *ApJ*, 206, 128
23. Dejonghe H., Merritt D., 1992, *ApJ*, 391, 531
24. Djorgovski S.G., Gal R.R., McCarthy J.K., Cohen J.G., De Carvalho R.R., Meylan G., Bendinelli O., Parmeggiani, G., 1997, *ApJ*, 474, L19
25. Djorgovski S.G., King I.R., 1986, *ApJ*, 305, L61
26. Einsel C., Spurzem R., 1999, *MNRAS*, 302, 81
27. Giersz M., Heggie D.C., 1993, *MNRAS*, 268, 257
28. Gnedin O.Y., Ostriker J.P., 1997, *ApJ*, 474, 223
29. Goodman J., 1987, *ApJ*, 313, 576
30. Grillmair C.J., Freeman K.C., Irwin M., Quinn P.J., 1995, *AJ*, 109, 2553
31. Guhathakurta P., Yanny B., Schneider D.P., Bahcall J.N., 1996, *AJ*, 111, 267
32. Gunn J.E., Griffin R.F., 1979, *AJ*, 84, 752
33. Gurzadyan V.G., Savvidi G.K., 1984, *Sov. Phys. Dokl.*, 29, 520
34. Gurzadyan V.G., Savvidy G.K., 1986, *A&A*, 160, 203
35. Heggie D.C., Ramamani N., 1989, 237, 757
36. Hénon M., 1961, *Ann. d'Astrophys.*, 24, 369
37. Hénon M., 1965, *Ann. d'Astrophys.*, 28, 62
38. Hut P., Makino J., 1999, *Science*, 283, 501
39. Illingworth G., 1976, *AJ*, 204, 73
40. Inagaki S., Wiyanto P., 1984, *PASJ*, 36, 391
41. Jablonka P., Bridges T.J., Sarajedini A., Maeder A., Meynet G., 1999, *ApJ*, 518, 627
42. Jablonka P., Courbin F., Meylan G., Sarajedini A., Bridges T.J., Magain P., 2000, *ApJ*, submitted
43. James R.A., 1977, *J. Comput. Phys.* 25, 71
44. Jeans J.H., 1913, *MNRAS*, 74, 109
45. Jeans J.H., 1915, *MNRAS*, 76, 70
46. Johnston K.V., Sigurdsson S., Hernquist L., 1999, *MNRAS*, 302, 771
47. Kandrup H.E., Willmes D.E., 1994, *A&A*, 283, 59
48. Kim C.-H., Chun M.-S., Min K.W., 1992, *As&SS*, 196, 191
49. King I.R., 1966, *AJ*, 71, 64
50. King I.R., 1981, *QJRAS*, 22, 227
51. Kormendy J., 1985, *ApJ*, 295, 73

52. Lauer T.R., Holtzman J.A., Faber S.M., et al., 1991, ApJ, 369, L45
53. Leon S., Meylan G., Combes F., 2000, A&A, submitted
54. Lupton R.H., Gunn J., 1987, AJ, 93, 1106
55. Lynden-Bell D., Wood R., 1968, MNRAS, 138, 495
56. Makino J., 1996a, in Dynamical Evolution of Star Clusters: Confrontation of Theory and Observations, IAU Symp. 174, eds. Hut P. & Makino J. (Dordrecht: Kluwer), p. 141 and p. 151
57. Makino J., 1996b, ApJ, 471, 796
58. Mayor M., Meylan G., Udry S., Duquenois A., Andersen J., Nordström B., Imbert M., Maurice E., Prévot L., Ardeberg A., Lindgren H., 1997, AJ, 114, 1087
59. Meylan G., Heggie D.C., 1997, A&AR, 8, 1-143
60. Meylan G., Mayor M., 1986, A&A, 166, 122
61. Meylan G., Mayor M., Duquenois A., Dubath P., 1995, A&A, 303, 761
62. Meylan G., Sarajedini A., Jablonka P., Djorgovski S.D., Bridges T.J., Rich R.M., 2000, ApJ, in preparation
63. Merritt D., 1993a, ApJ, 413, 79
64. Merritt D., 1993b, in Structure, Dynamics and Chemical Evolution of Elliptical Galaxies, ed. I. J. Danziger, W. W. Zeilinger & K. Kjær (ESO: Munich), 275
65. Merritt, D. 1996, AJ, 112, 1085
66. Merritt D., Meylan G., Mayor M., 1997, AJ, 114, 1074-1086
67. Murali C., Weinberg M.D., 1997, MNRAS, 291, 717
68. Murphy B.W., Cohn H.N., 1988, MNRAS, 232, 835
69. Norris J.E., Freeman K.C., Mayor M., Seitzer P., 1997, ApJ, 487, L187
70. Oh K.S., Lin D.N.C., 1992, ApJ, 386, 519
71. Pfenniger D., 1986, A&A, 165, 74
72. Portegies Zwart S.F., Makino J., McMillan S.L.W., Hut P., 1999, A&A, 348, 117
73. Resnikoff H.L., Wells R.O., 1998, Wavelet Analysis, Springer, Berlin Heidelberg
74. Rich R.M., Mighell K., Freedman W., Neill J.D., 1996, AJ, 111, 768
75. Salpeter E.E., 1955, ApJ, 121, 161
76. Slezak E., Durret F., Gerbal D., 1994, AJ, 108, 1996
77. Sosin C., King I.R., 1996, in Dynamical Evolution of Star Clusters: Confrontation of Theory and Observations, IAU Symp. 174, eds. Hut P. & Makino J. (Dordrecht: Kluwer), p. 343
78. Spitzer L., 1940, MNRAS, 100, 396
79. Spitzer L., 1969, ApJ, 158, L139
80. Spitzer L., 1987, Dynamical Evolution of Globular Clusters, (Princeton:

Princeton University Press)

81. Spitzer L., Chevalier R.A., 1973, ApJ, 183, 565
82. Spurzem R., 1998, in Dynamics of Galaxies and Galactic Nuclei, Eds. W.J. Duschl & C. Einsel, (ITA: Heidelberg), p. 271
83. Spurzem R., Aarseth S.J., 1996, MNRAS, 282, 19
84. Sugimoto D., Bettwieser E., 1983, MNRAS, 204, 19P
85. Takahashi K., 1995, PASJ, 47, 561
86. Trager S.C., King I.R., Djorgovski S.G., 1995, AJ, 109, 218
87. Vesperini E., 1992a, Europhys. Lett., 17, 661
88. Vesperini E., 1992b, A&A, 266, 215
89. von Hoerner S., 1960, Z. f. A., 50, 184
90. Yanny B., Guhathakurta P., Bahcall J.N., Schneider D.P., 1994, AJ, 107, 1745